Polycrystalline GeSn thin films on Si formed by alloy evaporation

2015 Appl. Phys. Express 8 061301

(http://iopscience.iop.org/1882-0786/8/6/061301)

Applied Physics Express **8**, 061301 (2015)
http://dx.doi.org/**10.7567/APEX.8.061301**

Polycrystalline GeSn thin films on Si formed by alloy evaporation

Munho Kim[1], Wenjuan Fan[1], Jung-Hun Seo[1], Namki Cho[1], Shih-Chia Liu[2], Dalong Geng[3], Yonghao Liu[2], Shaoqin Gong[4], Xudong Wang[3], Weidong Zhou[2], and Zhenqiang Ma[1]*

[1]*Department of Electrical and Computer Engineering, University of Wisconsin–Madison, Madison, WI 53706, U.S.A.*
[2]*Department of Electrical Engineering, NanoFAB Center, University of Texas at Arlington, Arlington, TX 76019, U.S.A.*
[3]*Department of Materials Science and Engineering, University of Wisconsin–Madison, Madison, WI 53706, U.S.A.*
[4]*Department of Biomedical Engineering and Wisconsin Institute for Discovery, University of Wisconsin–Madison, Madison, WI 53706, U.S.A.*
E-mail: mazq@engr.wisc.edu

Received March 2, 2015; accepted April 21, 2015; published online May 13, 2015

Polycrystalline GeSn thin films on Si substrates with a Sn composition up to 4.5% have been fabricated and characterized. The crystalline structure, surface morphology, and infrared (IR) absorption coefficient of the annealed GeSn thin films were carefully investigated. It was found that the GeSn thin films with a Sn composition of 4.5% annealed at 450 °C possessed a desirable polycrystalline structure according to X-ray diffraction (XRD) analyses and Raman spectroscopy analyses. In addition, the absorption coefficient of the polycrystalline GeSn thin films in the IR region was significantly better than that of the single crystalline bulk Ge. © 2015 The Japan Society of Applied Physics

The semiconducting, metastable GeSn alloy with a diamond-cubic structure has attracted considerable attention because of its tunable (direct) band gap, which is desirable for group IV-based photonic and infrared optoelectronic systems.[1,2] However, incorporating Sn into the Ge lattice has been a challenging task owing to the large lattice mismatch (~14.7%) between the two elements (α-Sn, $a_0 = 0.64892$ nm; Ge, $a_0 = 0.56579$ nm) and lower surface free energy of Sn with respect to Ge, leading to the surface segregation of Sn.[3,4] Moreover, owing to the limited bulk solubility of Sn in Ge, it is very difficult to form metastable GeSn alloys with a high Sn content. Consequently, nonequilibrium growth techniques such as low-temperature molecular beam epitaxy (MBE), chemical vapor deposition (CVD), RF sputtering, and thermal coevaporation of Ge and Sn via physical vapor deposition (PVD) have been used to form single crystalline $Ge_{1-x}Sn_x$ films.[4–7] However, methods of preparing the single crystalline GeSn films require a careful control of growth conditions to achieve high structural quality. In contrast, polycrystalline GeSn thin films with a high Sn concentration can offer a more economical and practical pathway toward optoelectronic applications with decent material properties.

In this work, we report on the formation of polycrystalline $Ge_{1-x}Sn_x$ films with a Sn concentration of up to 4.5% by thermal evaporation. The uniqueness of our approach is that we first form an amorphous GeSn film by GeSn alloy evaporation and then transform the amorphous GeSn film to a polycrystalline GeSn film by annealing. During the thermal annealing, the amorphous as-deposited GeSn thin film underwent solid-phase crystallization (SPC) and was subsequently transformed into the polycrystalline GeSn thin film. By analyzing the composition, crystalline structure, and optical characteristics of the annealed GeSn thin film, we found that the GeSn thin film annealed at 450 °C possessed the highest Sn composition of 4.5% and the most desirable polycrystalline structure since it exhibited the least XRD peak intensities for β-Sn and SnO_2. In addition, the absorption coefficient of the polycrystalline GeSn thin film at the IR region is significantly improved in comparison with that of the single crystalline Ge. Therefore, our approach enables the fabrication of a GeSn thin film with favorable polycrystalline quality and absorption coefficient, which can be potentially integrated into high-performance infrared optoelectronics.

Si(100) substrates were chemically cleaned with hydrofluoric acid (HF 49%) to acquire a native oxide-free Si surface and immediately loaded into a deposition chamber. No additional surface treatment on Si substrates was performed prior to the deposition. The GeSn layer was deposited from GeSn alloy pallets that contain 10% Sn on a Si substrate at a base pressure of $\sim 2 \times 10^{-7}$ Torr without the need of heating the substrate. Two deposition rates were applied to deposit 250-nm-thick GeSn thin films, namely, 5 nm/s (fast) and 0.5 Å/s (slow). An evaporated amorphous Ge thin film on a Si substrate with the same thickness was also prepared as a reference. After the GeSn deposition, samples were diced into 5×5 mm^2 pieces and annealed by rapid thermal annealing (RTA) in nitrogen ambient at various temperatures (from 100 to 600 °C at 50 °C increments). Because the melting temperature of Sn (230 °C) is lower than the crystallization temperature of GeSn, it is worthwhile to investigate the annealing effect on the deposited GeSn thin film. High-resolution X-ray diffraction (HR-XRD; Bruker D8 Discover diffractometer) and Raman spectroscopy were used to characterize the crystalline structure and Sn composition of the thin film. The surface morphologies of the as-deposited and annealed GeSn thin films were examined by atomic force microscopy (AFM; Park Systems). The optical properties of the 250-nm-thick 450 °C-annealed GeSn thin film, 600 °C-annealed Ge thin film, and bulk Ge, which is a single crystal, were measured using an ellipsometer (J. J. Woollam M-2000 DI) at wavelengths ranging from 300 to 1700 nm.

The crystalline structure of the as-deposited (i.e., prior to the annealing step) GeSn films on Si substrates was analyzed by XRD. As discussed below, our studies found that in order to achieve desirable polycrystalline GeSn films through SPC, the as-deposited GeSn films must have an amorphous structure. To establish the correlation between the deposition rate and the structure of the as-deposited GeSn thin films, GeSn films were deposited using two different deposition rates ("fast" and "slow"), as mentioned above. Figure 1(a) shows the XRD patterns for the GeSn films deposited with the slow and fast deposition rates, and the reference polycrystalline Ge film annealed at 600 °C. There was no visible peak detected from the GeSn thin film deposited at 5 nm/s, indicating that the GeSn thin film deposited at a fast deposition rate was amorphous. This is due to the fact that at a fast deposition rate, clusters of the deposited atoms do not have sufficient

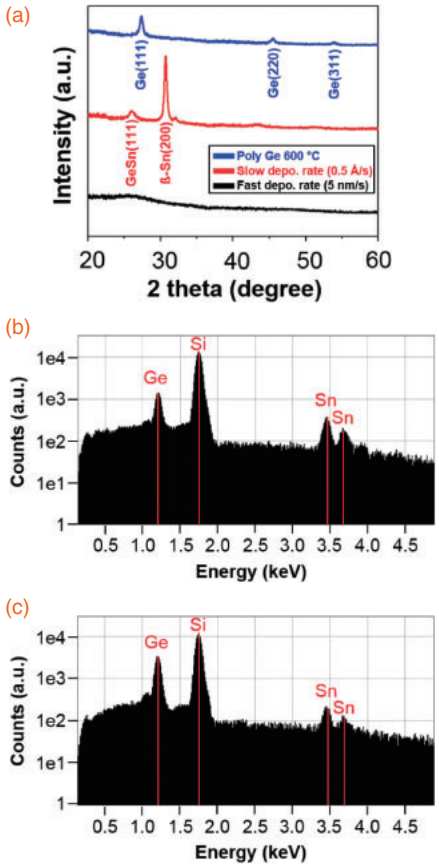

Fig. 1. (a) XRD patterns of the as-deposited GeSn thin films prepared at fast and slow deposition rates and the polycrystalline Ge film annealed at 600 °C. (b) EDS spectra taken from the GeSn deposited at a slow rate (0.5 Å/s). (c) EDS spectra taken from the GeSn deposited at a fast rate (5 nm/s).

time to form crystalline nuclei before they are surrounded by adjacent atoms.[8] In contrast, the slowly deposited GeSn film had a strong (200) β-Sn diffraction peak as well as a weak (111) GeSn peak, suggesting that β-Sn became the dominant crystalline phase during the deposition. This finding indicates that a slow deposition rate provided a sufficient amount of time for phase separation and the formation of the crystalline structure and thus was not the proper deposition condition to form amorphous GeSn films.

We performed energy-dispersive X-ray spectroscopy (EDS) analysis on the GeSn thin films formed by fast and slow deposition rates to study the chemical composition of the deposited films. As shown in Figs. 1(b) and 1(c), the EDS spectra revealed that both types of GeSn thin films showed the Ge peak and the Sn peak. The Si peaks came from the Si substrates. The peak intensity of Ge from the slowly deposited film was lower than that from the rapidly deposited film. On the other hand, the peak intensity of Sn from the slowly deposited film was higher than that from the rapidly deposited film. The strong Sn peak from the slowly deposited film is consistent with the dominant crystalline phase of (200) β-Sn, as shown in Fig. 1(a).

In order to investigate the crystalline structure changes of the GeSn thin films induced by annealing, the samples were annealed by RTA from 100 to 600 °C at 50 °C increments in nitrogen ambient for 5 min. Note that such a relatively short annealing time was sufficient to complete the transformation from an amorphous GeSn to a polycrystalline GeSn, owing to its rapid nucleation and growth kinetics.[9] Figure 2(a) shows the XRD patterns of the annealed GeSn thin films. There were no noticeable GeSn peaks for the GeSn films annealed at a temperature of up to the 250 °C, indicating that these films retained their amorphous structures. Because a Sn-rich liquid phase exists with a Ge-rich solid phase above 230 °C, it allows for the rearrangement of the atoms and thus nucleation leading to the formation of the polycrystalline GeSn structure. Annealing temperatures below 250 °C were not sufficient to acquire the Sn-rich liquid phase and thus failed to form crystalline nuclei. GeSn films annealed at 300–400 °C show four peaks corresponding to the following four diffraction peaks: (111) GeSn, (200) β-Sn, (220) GeSn, and (311) GeSn.[9] The strong β-Sn XRD peak implies that Sn segregated from the GeSn became the dominant crystalline phase in the GeSn thin film. The intensities of the (200) and (101) β-Sn peaks decreased significantly as the annealing temperature increased above 400 °C. The GeSn films annealed at 450–600 °C showed a (200) SnO_2 peak at 38.3°. Considering that the SnO_2 peak appeared at samples annealed at or above 500 °C, it is suggested that the segregated Sn on the surface was oxidized during high-temperature annealing. Note that the (200) β-Sn peak disappeared after the sample was annealed at or above 450 °C because β-Sn was oxidized and formed SnO_2, as evidenced by the appearance of the (200) SnO_2 peak.

Figure 2(b) shows the zoomed-in XRD patterns on the (111) GeSn peak. The GeSn film annealed at 400 °C had a clear (111) GeSn peak at 27.06°, and the peak gradually shifted to a higher diffraction angle as the annealing temperature increased. The (111) GeSn peak position of the sample annealed at 600 °C was shifted by 0.18 to 27.24°. This shift suggests that high-temperature annealing induced a tensile strain in the GeSn thin film. Figure 2(c) shows the XRD scan of the GeSn thin film annealed at 450 °C and that of the Ge annealed at 600 °C. Three diffraction peaks associated with GeSn were detected at 2θ of 27.17, 45.08, and 53.52° corresponding to the (111), (220), and (311) planes, respectively. All of the XRD GeSn peaks were shifted slightly to a lower diffraction angle when compared with the corresponding Ge XRD peaks. The built-in strain values in the GeSn and Ge thin films were extracted according to the thermal expansion coefficients of GeSn (~8% Sn), Ge, and Si, which are considered linear within our annealing temperature range, namely, $\sim 9 \times 10^{-6}$, $\sim 6 \times 10^{-6}$, and $\sim 3 \times 10^{-6}$ $°C^{-1}$, respectively.[10] Considering the different thermal expansion properties of GeSn, Ge, and Si, approximately 0.3% of the thermally induced tensile strain was expected in the GeSn film on a Si substrate upon cooling from 450 °C to room temperature. Such biaxial tensile strain caused the XRD peaks to shift to a higher diffraction angle, as shown in Fig. 2(c). Although the GeSn film had a larger thermally induced tensile strain, the GeSn XRD peak [(111) GeSn: 27.17°] was detected at slightly lower angles compared with the Ge peaks [(111) Ge: 27.38°]. This implies that the effect of Sn alloying exceeded the thermally induced tensile strain. The Sn concentration in the GeSn thin film can be calculated according to Vegard's law on the basis of the lattice constant of GeSn, which was extracted from the XRD analysis:

$$a_0^{Ge_{1-x}Sn_x} = a_0^{Ge}(1-x) + a_0^{Sn}x + b^{GeSn}x(1-x). \quad (1)$$

Here, a_0 is the lattice constant, x is the Sn concentration, and b is the bowing parameter ($b = -0.256$ Å).[11,12] The GeSn

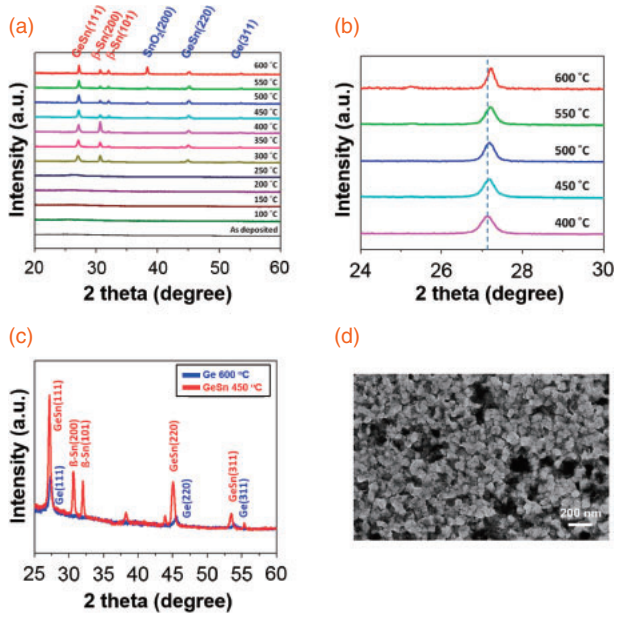

Fig. 2. (a) XRD patterns of the GeSn thin films annealed at various temperatures ranging from 100 to 600 °C at 50 °C increments. (b) XRD patterns of the GeSn thin films annealed from 400 to 600 °C, which focused on the GeSn {111} plane. (c) Comparison of the XRD patterns between the GeSn films annealed at 450 °C and the Ge substrate annealed at 600 °C. (d) SEM image taken from the surface of the GeSn film annealed at 450 °C.

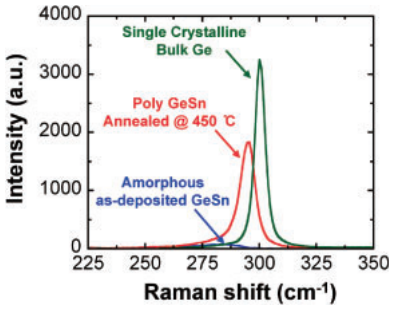

Fig. 3. Raman spectra taken from the single crystalline Ge substrate, as-deposited GeSn film, and GeSn film annealed at 450 °C.

thin film annealed at 450 °C had a strong (111) GeSn peak at 2θ of 27.17°. The out-of-plane lattice constant of GeSn was calculated to be 5.685 Å, according to Bragg's law. Using the lattice constant of GeSn (i.e., 5.685 Å) in Eq. (1), the Sn concentration was calculated to be 4.5%.

Figure 2(d) shows the scanning electron microscopy (SEM) image taken from the surface of the GeSn thin film annealed at 450 °C. It was found that the grain size of the GeSn was approximately 100 nm. It is speculated that our polycrystalline GeSn thin film has a higher optical absorption coefficient than a single crystalline GeSn owing to the scattering effect at the grain boundary.[13] On the other hand, the electrical resistivity of the polycrystalline GeSn thin film might be lower than that of the single crystalline GeSn, since grain boundaries generate holes in Ge-based semiconductors.[14]

The strain in the GeSn film annealed at 450 °C and its Sn concentration were further studied using Raman spectroscopy. We used a Horiba LabRAM ARAMIS Raman confocal microscope with a 100× objective and a He–Ne (632.8 nm) laser. Figure 3 shows the comparison of the Raman peaks of the GeSn sample annealed at 450 °C and the single crystalline (SC) Ge film. The Ge–Ge vibration mode peak of the SC Ge film appeared at 300.1 cm^{-1}, while the GeSn film annealed at 450 °C had its Ge–Ge peak at 295.6 cm^{-1}. As such, there was a 4.5 cm^{-1} shift in the Ge–Ge Raman peaks. The Sn concentration in the resulting GeSn film can be extracted from the Raman shift by eliminating the effect of the thermally induced tensile strain. 0.3% of the biaxial tensile strain could cause the Ge–Ge peak to shift approximately 1.2 cm^{-1} in wavenumber according to the following equation:[15]

$$\omega_{\text{Ge–Ge}} = \omega_0 - 400\varepsilon_{\parallel}, \quad (2)$$

where ω_0 is the Ge–Ge peak wavenumber in the case of no strain and $\varepsilon_{\parallel}$ is the biaxial strain in Ge. The amount of Ge–Ge peak shift (3.3 cm^{-1}) caused by the GeSn alloying was calculated by subtracting the shift (1.2 cm^{-1}) caused by the biaxial tensile strain from the total Ge–Ge peak shift (4.5 cm^{-1}) observed in the GeSn thin film, and the Sn composition in the GeSn film was calculated to be 4.5%.[16] The Sn concentration calculated from the Raman spectrum agrees well with that calculated from the XRD data (i.e., 4.5%).

The surface morphologies of the as-deposited and annealed GeSn thin films were investigated by AFM. Figure 4 shows the AFM images taken from the surfaces of the GeSn thin films obtained under various conditions: (a) as-deposited, (b) annealed at 300 °C, (c) annealed at 450 °C, and (d) annealed at 600 °C. The cross-sectional height profile of each two-dimensional (2D) AFM image along the red line (left side) is shown at the bottom of each 2D AFM image. The corresponding 3D AFM images (right side) also show the surface morphologies with a scanned area of $5 \times 5\,\mu m^2$. The root-mean-squared (RMS) surface roughness of the as-deposited GeSn was 0.638 nm, and the RMS surface roughness of the annealed GeSn films increased to 3.735, 8.393, and 13.584 nm upon annealing at 300, 450, and 600 °C, respectively. The height variation of the as-deposited sample was around 2 nm across the scanned area, which was less than 1% of the total thickness, while it increased to approximately 12, 30, and 40 nm in the 300-, 450-, and 600-°C-annealed samples due to protruding crystallites.

The optical properties of the 250-nm-thick 450-°C-annealed GeSn thin film, the 600-°C-annealed Ge thin film, and bulk Ge were measured using an ellipsometer. Figure 5 shows the absorption coefficients of the three samples plotted as a function of wavelength. From 600 to 1700 nm, the absorption coefficients of the 450-°C-annealed polycrystalline GeSn thin film and the 600-°C-annealed polycrystalline Ge thin film on a Si substrate were consistently higher than that of the bulk Ge. Furthermore, while the absorption coefficient of the bulk Ge showed an abrupt reduction at a wavelength longer than 1550 nm, the 450-°C-annealed polycrystalline GeSn thin film on a Si substrate maintained a relatively high absorption coefficient (on the order of 10^5 to 10^6 cm^{-1}) compared with that of the single crystalline GeSn reported in Ref. 7 within the same wavelength range. In addition, the absorption coefficient of the GeSn thin film was higher than that of the Ge thin film formed by SPC. The absorption coefficient (α) of the thin film is related to the "k" value by the equation: $\alpha = (4 \times \pi \times k)/\lambda$.[17] As investigated by Kasper et al.,[17] the k value of the $Ge_{1-x}Sn_x$ film increases as the Sn composition increases. Thus, the difference in the absorption coefficients in the GeSn thin film was clearly due to the Sn-doping effects. Such a

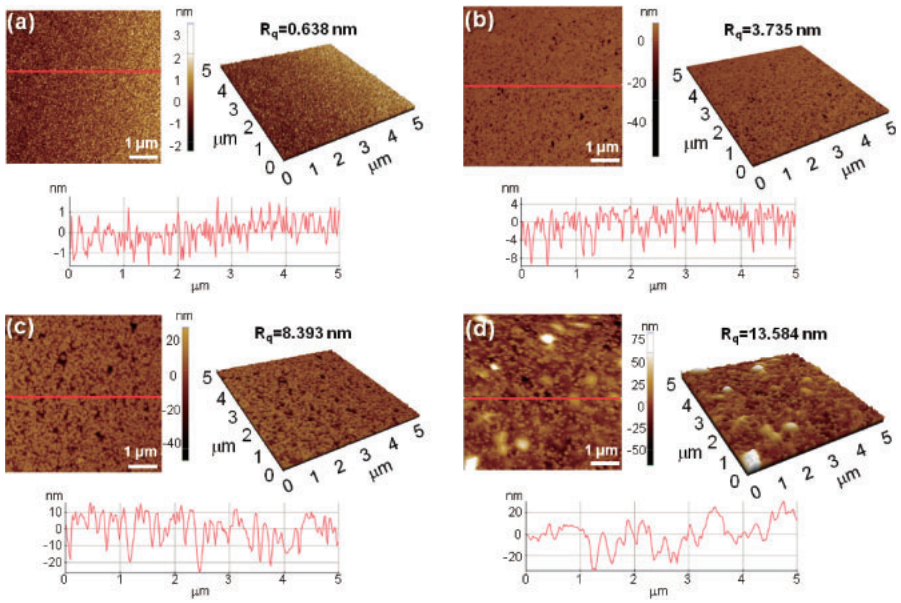

Fig. 4. AFM images of the 250-nm-thick GeSn films (a) as-deposited, (b) annealed at 300 °C, (c) annealed at 450 °C, and (d) annealed at 600 °C. The scale bar in AFM images indicates 1 μm. Their RMS surface roughness values are 0.638, 3.735, 8.393, and 13.584 nm, respectively.

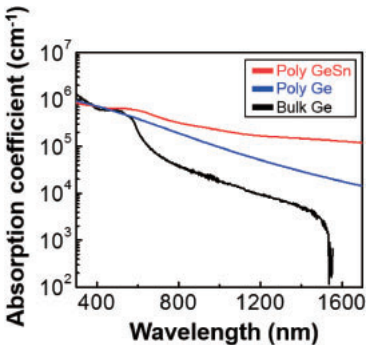

Fig. 5. Absorption coefficients of the GeSn thin film annealed at 450 °C, Ge thin film annealed at 600 °C, and single crystalline bulk Ge substrate at the wavelength ranging from 300 to 1700 nm.

high absorption coefficient could be attributed to the narrowed bandgap of the polycrystalline GeSn resulting from the high Sn concentration, as well as the grain boundaries, which produce scattered light that was subsequently reabsorbed by the material. Overall, the polycrystalline GeSn thin film showed 10 times higher absorption coefficient at the wavelength range of 900–1500 nm and 100 times higher at wavelengths of 1550 nm or above, than that of the bulk Ge substrate, which is very promising for IR light detection.

Polycrystalline GeSn thin films were prepared by the thermal evaporation of GeSn alloy followed by thermal annealing. The effects of deposition rates and annealing temperature on the structure and morphology of the GeSn films were characterized by XRD, Raman spectroscopy, and AFM. The as-deposited GeSn thin films formed at a high deposition rate were amorphous, which were successfully transformed into a polycrystalline structure during the high-temperature (300 to 600 °C) annealing via SPC. The GeSn thin films annealed at 450 °C showed the highest Sn composition of 4.5% and good polycrystalline quality as the XRD peak intensities of β-Sn and SnO_2 were very weak. In addition, the absorption coefficient of the GeSn at the IR region was significantly improved in comparison with that of the bulk Ge. The enhanced absorption coefficient of the polycrystalline GeSn film makes it a promising material for high-performance IR optoelectronic applications.

Acknowledgments This work was supported by a PECASE award from AFOSR under grant No. FA9550-09-1-0482. The program manager at AFOSR is Dr. Gernot Pomrenke.

1) S. Gupta, B. Magyari-Kope, Y. Nishi, and K. C. Saraswat, J. Appl. Phys. **113**, 073707 (2013).
2) G. He and H. A. Atwater, Phys. Rev. Lett. **79**, 1937 (1997).
3) O. Gurdal, R. Desjardins, J. R. A. Carlsson, N. Taylor, H. H. Radamson, J. E. Sundgren, and J. E. Greene, J. Appl. Phys. **83**, 162 (1998).
4) H. Pérez Ladrón de Guevara, A. G. Rodríguez, H. Navarro-Contreras, and M. A. Vidal, Appl. Phys. Lett. **83**, 4942 (2003).
5) J. Werner, M. Oehme, M. Schmid, M. Kaschel, A. Schirmer, E. Kasper, and J. Schulze, Appl. Phys. Lett. **98**, 061108 (2011).
6) B. Vincent, F. Gencarelli, H. Bender, C. Merckling, B. Douhard, D. H. Petersen, O. Hansen, H. H. Henrichsen, J. Meersschaut, W. Vandervorst, M. Heyns, R. Loo, and M. Caymax, Appl. Phys. Lett. **99**, 152103 (2011).
7) R. R. Lieten, J. W. Seo, S. Decoster, A. Vantomme, S. Peters, K. C. Bustillo, E. E. Haller, M. Menghini, and J.-P. Locquet, Appl. Phys. Lett. **102**, 052106 (2013).
8) I. T. H. Chang, B. Cantor, and A. G. Cullis, J. Non-Cryst. Solids **117**, 263 (1990).
9) H. Li, J. Brouillet, A. Salas, X. Wang, and J. Liu, Opt. Mater. Express **3**, 1385 (2013).
10) R. Roucka, Y.-Y. Fang, J. Kouvetakis, A. V. G. Chizmeshya, and J. Menendez, Phys. Rev. B **81**, 245214 (2010).
11) F. Gencarelli, B. Vincent, J. Demeulemeester, A. Vantomme, A. Moussa, A. Franquet, A. Kumar, H. Bender, J. Meersschaut, W. Vandervorst, R. Loo, M. Caymax, K. Temst, and M. Heyns, ECS J. Solid State Sci. Technol. **2**, P134 (2013).
12) H. Li, Y. X. Cui, K. Y. We, W. K. Tseng, H. H. Cheng, and H. Chen, Appl. Phys. Lett. **102**, 251907 (2013).
13) P. Fulay and J.-K. Lee, *Electronic, Magnetic, and Optical Materials* (CRC Press, Boca Raton, FL, 2010).
14) K. Toko, I. Nakao, T. Sadoh, T. Noguchi, and M. Miyao, Solid-State Electron. **53**, 1159 (2009).
15) P. H. Tan, K. Brunner, D. Bougeard, and G. Abstreiter, Phys. Rev. B **68**, 125302 (2003).
16) V. R. D'Costa, J. Tolle, R. Roucka, C. D. Poweleit, J. Kouvetakis, and J. Menéndez, Solid State Commun. **144**, 240 (2007).
17) E. Kasper, M. Kittler, M. Oehme, and T. Arguirov, Photonics Res. **1**, 69 (2013).